A Computational Study of Regioselectivity in a Cyclodextrin-Mediated Diels–Alder Reaction: Revelation of Site Selectivity and the Importance of Shallow Binding and Multiple Binding Modes

Wan-Sheung Li,[a] Wen-Sheng Chung,*[b] and Ito Chao*[a]

Abstract: The use of a cyclodextrin·Diels–Alder transition structure complex (CD·TS) as a model in molecular dynamics simulations has enabled us to gain insight into the controlling factors in the cyclodextrin-mediated Diels–Alder reaction of methyl-*p*-benzoquinone with isoprene. MD simulations were carried out with multiple binding configurations of the CD·TS (TS = *meta*-TS, *para*-TS) complexes at the top and bottom rims of β-CD. We discovered that i) only shallow binding with the CD is necessary for the regioselectivity, and multiple binding geometries are possible; ii) the narrow bottom rim, with the primary hydroxyl groups, of the CD binds both regio-TSs better than at the wider top rim (secondary hydroxyl groups), which was unexpected from the perspective of shape complementarity that governs the stability of most CD·guest complexes. Overall, the bottom rim of the CD exhibits higher regioisomer discrimination for the *meta*-TS; iii) structural clustering analyses of the CD·TS configurations (sampled during MD simulations) have enabled us to evaluate the binding energies of the different binding configurations. The result indicates that there is a direct correlation between *meta*-product selectivity and a higher number of binding configurations favoring the formation of the CD·*meta*-TS complex. The main forces of stabilization in the CD·TS complexes are the van der Waals interactions when the TS is bound at the top rim. At the bottom rim, closer contacts between polar functional groups of the TS and CD have increased the importance of electrostatic interactions. We found that van der Waals, solvation, and torsional forces are less favorable for complexation at the bottom rim; however, this is compensated by large favorable electrostatic interactions. With insights obtained from the study of CD·TS complexes and MD simulations of the modified heptakis-[6-*O*-(2-hydroxy)propyl]-β-CD, we were able to explain why a low selectivity was observed when the Diels–Alder reaction was carried out in this modified CD. Two types of search method [Monte Carlo and multiple minimum (MCMM) and molecular dynamics (MD)] to explore and evaluate the different possible binding geometries of the TS within β-CD, were discussed.

Keywords: cycloadditions · cyclodextrin · molecular dynamics calculations · transition structure

Introduction

The potential use of cyclodextrins (CDs) as enzyme models to study organic catalytic reactions in biological systems is of considerable interest with respect to the understanding of reaction mechanisms in enzyme systems as well as interactions in host–guest inclusion complexes. CDs are cyclic oligosaccharides consisting of six or more α-(1,4)-linked glucose units, and the first three in the series, α, β and, γ are being extensively studied.[1] They are normally depicted as having a distinctive "bucket" geometry with a rigid and well-defined cavity. The secondary hydroxyl groups (top rim) are located around the wider opening of the cavity while the primary hydroxyl groups (bottom rim) are situated around the narrower end. The cavity itself is hydrophobic, and consists of methylene groups and glycosidic oxygen atoms. The many outward-pointing hydroxyl groups located around both openings of the cavity make cyclodextrins water-soluble.

A wide variety of techniques have been used to study the inclusion process. These range from spectroscopy, thermodynamics, chromatography, as well as X-ray and neutron diffraction methods, to the more recent theoretical calculations. The majority of the computational methods is based on force-field representations and employs molecular mechanics

[a] Prof. Dr. I. Chao, Dr. W.-S. Li
Institute of Chemistry
Academia Sinica
Taipei 11529 (Taiwan)
Fax: (886) 2-2783-1237
E-mail: ichao@chem.sinica.edu.tw

[b] Prof. Dr. W.-S. Chung
Department of Applied Chemistry
National Chiao-Tung University
Hsinchu 30050 (Taiwan)
E-mail: wschung@cc.nctu.edu.tw

Supporting information for this article is available on the WWW under http://www.chemeurj.org/ or from the author.

  0947-6539/03/0904-0951 $ 20.00+.50/0

and molecular dynamics simulations to study CD·guest inclusion complexes.[2–9] These include the evaluation of binding energies to gain insight into the inclusion process and prediction of guest orientation upon inclusion. Molecular modeling is also used to understand how molecular recognition takes place, especially in chromatography with a chiral stationary phase.[3d–f] Computational studies dealing with catalytic and chemical reactions in the presence of CD are rather limited. They are mainly focused on CD-catalyzed reactions of ester hydrolysis, and deacylation of acids and esters.[9] More recently, the role of CD in altering the course of stereochemical reactions was investigated by Jaime et al. They investigated the face selectivity of the photo[2+2]cycloaddition of 5-substituted adamantan-2-ones with furmaronitrile.[2e] In this example, face selectivity was achieved by the formation of a CD·adamantone complex, thus partially blocking the π-face *syn* to the adamantanone.

In this paper, we investigate the controlling factors that are responsible for the regioselectivity of the Diels–Alder reaction of methyl-*p*-benzoquinone (**1**) with isoprene in the presence of β-CD and modified β-CD, heptakis-[6-*O*-2-hydroxy)propyl]-β-CD (7-β-CD) (Scheme 1).[10a] The Diels–Alder reaction is frequently employed in the synthesis of cyclic organic compounds with fine control over the stereochemistry. A great deal of research has been focused on controlling the course of reaction by the use of aqueous solvents and in the presence of Lewis acid. Although aqueous solutions have been used for a long time, it was only in 1980 that Breslow and co-workers reported that intermolecular Diels–Alder reactions were affected in the presence of water and CDs.[4c] They showed that the rates of reaction of cyclopentadiene with butenone and acrylonitrile were dramatically increased in water, and the reaction rates were even faster in the presence of β-CD. However, reactions carried out in α-CD were found to be retarded compared with those in water. Breslow suggested that the origin of the acceleration in β-CD is a combination of a hydrophobic effect and the simultaneous inclusion of the diene and dienophile within the CD cavity. In an extreme case, CD can act as an inhibitor, as shown in the reaction of anthracene-9-carbinol and *N*-ethylmaleimide with α-CD where the CD cavity can only accommodate one guest molecule.[4] The importance of complex inclusion in the CD cavity was further reinforced by Sternbach and co-workers: they reported enhanced rates and product selectivities of intramolecular Diels–Alder reactions in a series of furan-dienes in aqueous solutions of β-CD but not in those containing α-CD.[4d]

Our study is focused on a more recent report by one of us, Chung et al., who showed that under different reaction conditions, the Diels–Alder reaction of methyl-*p*-benzoquinone with isoprene gave different preferred regioproducts (Scheme 1).[10a] In aqueous or organic solutions, the reactions gave almost equal ratios of the *para* and *meta* products with a slight preference for the *para* product. However, in the presence of β-CD, the *para*/*meta* ratio shifted to 14:86.[10a] The *meta*-TS has two methyl groups sticking out in nearly parallel directions, therefore, it has a bulky portion (see upper part of *meta*-TS in Scheme 2) and a less sterically demanding portion. With these shape characteristics of *meta*-TS, one would intuitively assume that the less sterically demanding lower portion is embedded into the CD cavity from the wider top rim with the two methyl substituent groups pointing out of the CD (Scheme 2). This simple model of the binding mode is

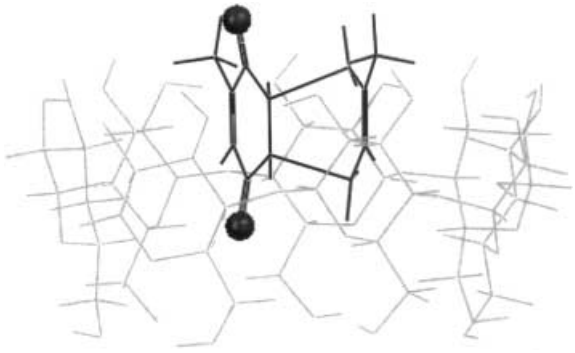

Scheme 2. A simple model showing a binding configuration which has good shape and size complementarities with the cavity of the β-CD of the CD·*meta*-TS complex.

attractive because a methyl group sticks out from the lower portion in *para*-TS, which would bump into the cavity wall and make the CD·*para*-TS less preferable than the CD·*meta*-TS. Therefore, it has been assumed that the product preference of this Diels–Alder reaction originates sterically in terms of "cavity size control" in the complexed transition state during adduct formation. A modified β-CD (7-β-CD) was also employed in the hope of gaining better product selectivity by deepening the hydrophobic cavity; however, the experimental results indicated only a very low selectivity.[10a]

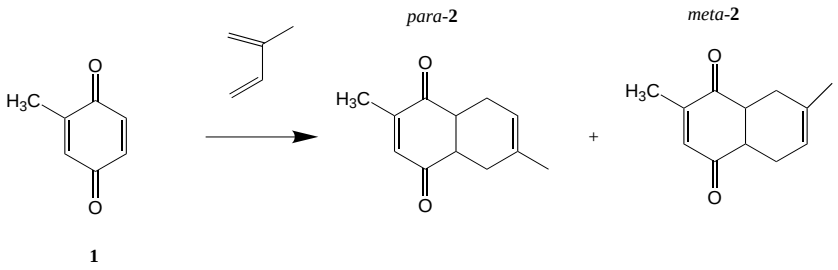

1

53:47 (acetone/toluene)
56:44 (water)
14:86 (β-CD/water)
45:55 (7-β-CD/water)

Scheme 1. Diels–Alder reaction of methyl-*p*-benzoquinone (**1**) with isoprene. The experimental product ratios of the reaction are also given.

To date, we have found only two attempts in the literature in which the CD·TS complexes of the Diels–Alder reaction are studied computationally.[5] In the communication by Mayoral and co-workers,[5a] the Diels–Alder reactions of cyclopentadiene and various dienophiles catalyzed by β-CD were studied by a semiempirical quantum

0947-6539/03/0904-0952 $ 20.00+.50/0 *Chem. Eur. J.* **2003**, *9*, No. 4

mechanical method and a simple Lennard–Jones potential. They modeled the CD·TS complexes by keeping both the guest and the CD rigid during the energy evaluation based on the simple Lennard–Jones potential. Important factors, such as solvation effect and the induced-fit effect of CD, were not considered. In a more recent study by Houk et al., one of these Diels–Alder reactions was studied in more detail with the aim of identifying the origins of noncovalent catalysis.[5c] In this paper, we explore and evaluate different possible low-energy binding configurations of the CD·reactant and CD·TS complexes without keeping the CD fixed, so that the induced-fit effect of CD can be incorporated. We use two search methods to search for low-energy configurations, namely, Monte Carlo multiple minimum (MCMM) and molecular dynamics (MD). The structures of the TS were obtained quantum mechanically and were kept rigid during the search. This simple approach with rigid guests revealed the effect of shape difference on complexation. Unlike many computational studies so far, we examined the binding behavior of the guest molecule in both the upper, secondary hydroxyl, and lower, primary hydroxyl, rims of the CD. The result proved to be highly valuable in the understanding of the complexation of a bulky guest molecule containing polar functional groups. The key issues we address in this paper are how the TS binds to the CD and how the selectivity is exerted. Our results can shed light on the position of the most selective binding site in this Diels–Alder reaction, and why product selectivity was not improved upon the modification of β-CD.[10a] Important factors, such as the forces responsible for the selectivity, are discussed.

Results and Discussion

Modeling of methyl-*p*-benzoquinone (1)·β-CD complex: In the first stage of the reaction, methyl-*p*-benzoquinone (**1**) was first added to a solution of excess cyclodextrin followed by the addition of the diene to prevent dimerization of the diene. Thus in the initial stage, an inclusion complex of the dienophile and CD was formed. The understanding of this inclusion process and the dynamic behavior of the guest molecule are highly important because these may give us some insights into how the CD can eventually alter the regioselectivity of the Diels–Alder reactions. How does the binding of the CD·dienophile complex affect an approaching diene, which then leads to the formation of the activated Diels–Alder complex? The result of our MD simulations of the CD·**1** complexation, starting from the two complexation configurations shown in Scheme 3, showed that the guest molecule is loosely bound in the CD cavity with it shuttling back and forth within the rims of the CD. It is possible that the reactive ene group is exposed either at the upper rim or the lower rim, depending on how **1** is inserted into the cavity.[11] Thus, an approaching diene can have the opportunity to attack at both ends allowing a Diels–Alder reaction to take place.

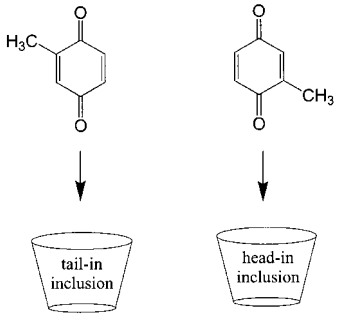

Scheme 3. The two docking orientations considered in the inclusion process of **1** in the 1:1 complexation.

Modeling of CD·*para*-TS and CD·*meta*-TS complexes

Searching for binding configurations with the MCMM method: In order to understand how selectivity was achieved through cavity size control in the complexed transition state during adduct formation, different possible orientations of the TS within the CD were assessed. They are designated as types **a**–**f** (Scheme 4). Our initial approach was to adopt a random movement search method by means of the MCMM procedure described in the Computational Methods. Although it was proved later on that this approach failed to rank the different guest binding configurations in the correct order, there are a few important observations worth mentioning. The results of these simulations are shown in Table 1, which lists the lowest energy structures of each configuration type found. The MCMM results showed that there is an overall preference for binding at the top rim than at the bottom rim of CD. This fits our initial model where the upper rim is wider, so to better accommodate the bulky TS. When we examined the energy of

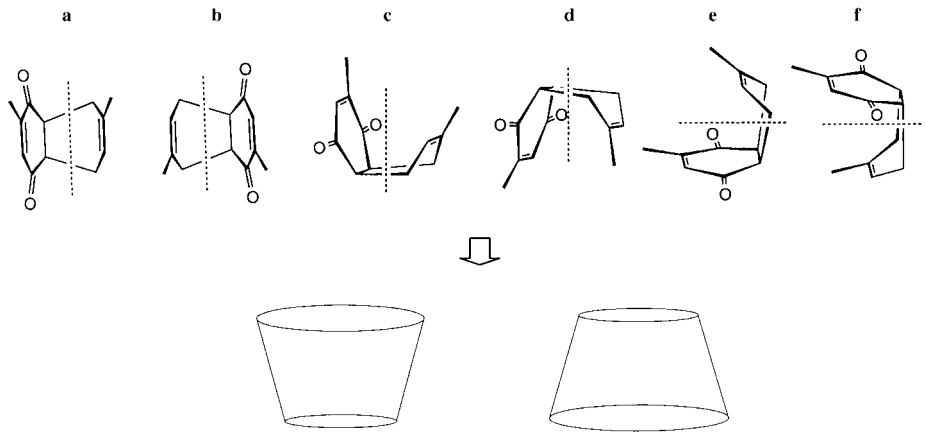

Scheme 4. Six docking TS configurations (**a**–**f**) at the top and bottom rims of β-CD as initial structures for MCMM and MD searches. Bonds intersecting with the dotted lines are the bonds that are being formed in the Diels–Alder TS. H atoms are omitted for clarity.

  0947-6539/03/0904-0953 $ 20.00+.50/0

Table 1. Energetic information of local minima [kJ mol^{-1}] obtained from MCMM conformational search and subsequent 30 ps MD simulations, of the CD·*para*-TS and CD·*meta*-TS complexes at the a) top, secondary hydroxyl, rim and b) bottom, primary hydroxyl, rim of CD.

		MCMM		MCMM-MD[a]	
	configuration type	ΔE_{bind}[b]	E_{CD}[b]	ΔE_{bind}[b]	E_{CD}[b]
top rim					
	CD·*para*-TS				
	a	−53.45	208.39	−70.04	189.52
	b	−46.77	228.96	_[d]	[d]
	c	−58.79	221.02	−75.59	207.80
	d	−53.00	239.05	−70.84	198.67
	e	−55.51	208.72	−74.14	198.06
	f	−59.21	219.24	−76.73	213.52
	CD·*meta*-TS				
	a	−54.29	237.44	−75.34	193.99
	b	[c]	[c]		
	c	−57.92	229.75	−74.39	209.51
	d	−51.08	244.89	−70.99	223.90
	e	−46.42	223.83	−70.10	198.23
	f	−59.89	219.17	−71.00	206.94
bottom rim					
	CD·*para*-TS				
	a	[c]	[c]		
	b	[c]	[c]		
	c	−34.60	258.48	−73.44	209.17
	d	−19.98	271.73	−82.19	206.75
	e	[c]	[c]	[d]	[d]
	f	−16.98	276.56	−72.04	199.15
	CD·*meta*-TS				
	a	[c]	[c]		
	b	[c]	[c]		
	c	−41.52	255.07	−75.85	221.68
	d	−22.35	266.40	−54.01	228.96
	e	[c]	[c]		
	f	−33.52	280.11	−79.50	235.41

[a] 30 ps MD simulation with 30 ps equilibration step at 273 K for the lowest energy structure of each configuration type found by the MCMM search. [b] $\Delta E_{bind} = E_{CD\cdot TS} - E_{free\ CD} - E_{free\ TS}$ (Note that E_{CD} is the single-point energy of the complexed CD geometry, whereas $E_{free\ CD}$ is from a full optimization of neutron diffraction CD). [c] Configuration type not found within the energy range examined. [d] Geometry changed during the 30 ps simulation.

the CD (E_{CD}) within the complexes, we noticed that, in general, E_{CD} for complexes binding at the bottom rim exhibit higher energy (see E_{CD} at the left-hand side of Table 1). As a consequence, this critically affected the calculated complexation binding energy (ΔE_{bind}), thus resulting in overall less stabilized CD·TS complexes binding at the bottom rim. An immediate question that springs to mind is: is this real or an artifact from our modeling? To answer this, we carried out short MD simulations (30 ps with a 30 ps equilibration step at 273 K) on each structure, so that the CD has a further chance to relax its structure, and collected structures at every 1 ps during the simulations. We found that simulations at 273 K were adequate to sample the structures while maintaining the configuration type. The collected structures were minimized. The lowest energy structure of each configuration type is shown alongside with the MCMM results in Table 1 (see under MCMM-MD). It can be seen that the binding preference between the two rims and the difference in E_{CD} are less obvious. When we checked the E_{CD} at different stages, we found that E_{CD} of each starting structure in the MCMM simulations are mostly within 10 kJ mol^{-1} of each other, except for a few top-rim binding structures where they showed much higher E_{CD}. After the MCMM search, the E_{CD}s are ≈50 kJ mol^{-1} lower in energy than the starting E_{CD} values for top-rim binding, whereas the E_{CD} values before and after the search are very similar for the bottom-rim binding. However, these E_{CD} values (for the bottom-rim binding) after the MCMM-MD were minimized to the energies comparable with the top rim MCMM-MD. These observations could be inherent from the search method in use and the nature of the CD. It seems that when binding takes place at the bottom rim, the energy barriers between the energy wells on the PES (potential energy surface) are much higher. Therefore, although we adopted a no-constraint-on-CD approach in the MCMM search, it did not incorporate the induced-fit effect of CD effectively. Our MCMM simulations highlight the downfall of the commonly adopted search procedure in which one presumes where and how a guest should bind, with the guest molecule docked into a desirable position and the energy minimized to the nearest minimum on the potential energy surface.

Searching for binding configurations with the molecular dynamics method: Because of the sampling problem we encountered from the MCMM search method, molecular dynamics simulations were used for further investigations. This approach not only facilitates the search of low energy configurations of CD complexes, but also provides statistically averaged binding energies. Lipkowitz et al.[3f] used the AMBER* force field to demonstrate that binding energies averaged over multiple trajectories of long-term simulation (nanosecond range) were able to reproduce the experimental elution order observed in gas chromatography for enantioselectivity achieved by stationary phase with permethyl-β-CD. In our case, we employed six guest configurations, illustrated in Scheme 4, as starting geometries for the MD simulations, each with 5 ns of simulation time. Table 2 gives the energy contribution of the complexation energy. The simulations predicted a binding preference for *meta*-TS, which agreed

Table 2. Energy contributions derived from complexation of the *para*- and *meta*-TS with β-CD docked at the top and bottom rims of CD. The energies were calculated by means of the mean values of individual energy contribution from the 5000 ps MD simulations in a continuum GB/SA water solvation model with six initial guest orientations.[a]

	Top rim		Bottom rim	
E [kJ mol^{-1}]	CD·*para*-TS	CD·*meta*-TS	CD·*para*-TS	CD·*meta*-TS
$\Delta\langle E_{bind}\rangle$	−36.91	−39.51	−39.25	−43.97
$\Delta\langle E_{vdw}\rangle$	−47.87	−49.74	−40.51	−44.72
$\Delta\langle E_{elec}\rangle$	−8.47	−7.56	−29.03	−32.22
$\Delta\langle E_{sol}\rangle$	22.77	21.35	27.79	31.17
$\Delta\langle E_{stretch}\rangle$	−0.31	0.35	−0.42	−0.02
$\Delta\langle E_{bend}\rangle$	−1.27	−0.81	−8.13	−8.40
$\Delta\langle E_{torsion}\rangle$	−2.62	−3.05	10.12	10.27

[a] The energy components $\Delta\langle E\rangle$ were calculated by subtracting the corresponding $\langle E\rangle$ with a standard $\langle E\rangle$ of free CD and $\langle E\rangle$ of TS. The $\langle E\rangle$ of free CD were calculated from a 1000 ps MD simulation, and $\langle E\rangle$ of both TS were from a 100 ps MD simulation. The MD simulations of these uncomplexed species were carried out at a constant temperature of 300 K with an equilibration step of 30 ps in a continuum GB/SA water solvation model.

0947-6539/03/0904-0954 $ 20.00+.50/0 *Chem. Eur. J.* **2003**, *9*, No. 4

with the observed regioselectivity of the *meta*-product.[10a] An unexpected finding is that, although the *meta*-TS is preferred at both the top and bottom rims of CD, it is the binding at the bottom rim which shows higher regioisomer discrimination [$\Delta\Delta\langle E_{bind}\rangle_{top} = -39.51 - (-36.91) = -2.60$ kJ mol^{-1} and $\Delta\Delta\langle E_{bind}\rangle_{bottom} = -43.97 - (-39.25) = -4.72$ kJ mol^{-1}]. In fact, the bottom rim of the CD exhibits higher binding ability for both TSs [$\Delta\Delta\langle E_{bind}\rangle_{para\text{-}TS} = -39.25 - (-36.91) = -2.34$ kJ mol^{-1} and $\Delta\Delta\langle E_{bind}\rangle_{meta\text{-}TS} = -43.97 - (-39.51) = -4.46$ kJ mol^{-1}]. Since the energy differences are not large, binding at both rims is possible. MD simulations were also carried out in the gas phase, where similar trends were observed but with larger energy differences; the higher binding ability of *meta*-TS compared to *para*-TS at the bottom rim [$\Delta\Delta\langle E_{bind}\rangle_{top} = -0.4$ kJ mol^{-1}, $\Delta\Delta\langle E_{bind}\rangle_{bottom} = -9.19$ kJ mol^{-1}], and higher binding ability for both TSs at the bottom rim [$\Delta\Delta\langle E_{bind}\rangle_{para\text{-}TS} = -13.60$ kJ mol^{-1}, $\Delta\Delta\langle E_{bind}\rangle_{meta\text{-}TS} = -22.39$ kJ mol^{-1}] (see the Supporting Information). Although these observations of bottom-rim preference are different from many examples of aqueous guest binding from NMR measurements where the binding is believed to take place at the wider top rim.[12] There are a few cases where bottom-rim binding of guests have been documented in aqueous solution.[13, 14] Indirect support of our own chemical systems for the possibility of bottom-rim binding in the transition state during adduct formation was obtained from ^{1}H NMR titration study of the complexed *meta* product, where upfield shifts of H3 ($\Delta\delta = 9.3$ Hz $= 0.031$ ppm), H5 ($\Delta\delta = 24.4$ Hz $= 0.081$ ppm) and H6 ($\Delta\delta = 5.8$ Hz $= 0.019$ ppm) of β-CD were observed.[10a] It is not surprising that of the two bottom rim hydrogen atoms, H5 is shifted upfield much more than H6; H5 is basically pointing into the cavity, whereas the position of H6 is much more mobile on account of the rotational freedom around the C5–C6 bond.

As mentioned previously, the simulations showed that the best binding site is at the bottom rim with the primary hydroxyl groups. It is important to find out the reasons for this preference. From Table 2, we have found that van der Waals interactions, solvation, and torsional forces are less favorable for complexation at the bottom than at the top rim of CD [for the CD·*para*-TS complex, $\Delta\Delta\langle E_{vdw}\rangle = 7.36$ kJ mol^{-1}, $\Delta\Delta\langle E_{sol}\rangle = 5.02$ kJ mol^{-1}, $\Delta\Delta\langle E_{torsion}\rangle = 12.74$ kJ mol^{-1}; for the CD·*meta*-TS, $\Delta\Delta\langle E_{vdw}\rangle = 5.02$ kJ mol^{-1}, $\Delta\Delta\langle E_{sol}\rangle = 9.82$ kJ mol^{-1}, $\Delta\Delta\langle E_{torsion}\rangle = 13.32$ kJ mol^{-1}]; however, these are compensated by large favorable electrostatic interactions and the bending energy [$\Delta\Delta\langle E_{elec}\rangle = -20.56$, $\Delta\Delta\langle E_{bend}\rangle = -6.86$ and $\Delta\Delta\langle E_{elec}\rangle = -24.66$, $\Delta\Delta\langle E_{bend}\rangle = -7.59$ kJ mol^{-1} for CD·*para*-TS and CD·*meta*-TS, respectively] (Table 2). This implies that, when a guest molecule contains polar functional group(s), such as C=O, hydrogen-bonding interactions with the primary hydroxyl groups could be an important factor in determining the overall complex stability. As an implicit water model was used in our simulations, we resorted to experimental findings to evaluate whether hydrogen bonding within a host–guest complex could indeed compete against hydrogen bonding between solute and water molecules in aqueous solutions, which is what our results had suggested. There are some experimental studies focusing on the contribution of hydrogen-bonding interactions in CD complexation in aqueous solution.[15–17] Ross and Rekharsky investigated pairs of structurally related aromatic guests, either with or without a phenolic OH group. They reported the increments in ΔH^0 and ΔG^0 in aqueous solution that were ascribed to hydrogen-bonding interaction involving the guest molecules and the hydroxyl groups of the CD.[15] Therefore, from the scenario provided by our simulations, we concluded that large favorable electrostatic interactions between the guest and the bottom rim of the CD is the source of the binding preference at the bottom rim.

The next question we need to address is: does "cavity size control" play a role in the selectivity? The long-range O4–O4 distances of the glycosidic oxygen atoms (e.g. glycosidic oxygens from the first to the forth pyranose units) and the glycosidic dihedral angles C1-O4′-C4′-C3′ (see Figure 2 for atomic labeling) were monitored during the MD simulations. Analyses of snapshots taken during the different simulations showed there are slight variations in the binding configuration space sampled from one simulation to another, and the length of time of the different binding configurations sampled also varied. However, we have observed that simulations with multiple initial configurations at the top rim, the majority (4 out of the 6 simulations) do exhibit a similar trend. In general, when the TS binds at the top rim, the glycosidic O4–O4 distances showed that the CD is more distorted in the CD·*meta*-TS complex (Figure 1), where it shows a greater difference in the preferred long-range distance of the 7 pairs of O4–O4 distances. In addition, mean O4–O4 distances of the 7 pairs of oxygen atoms are in the range 9.84–10.07 and 9.68–10.17 Å for CD·*para*-TS and CD·*meta*-TS, respectively. This correlates well with the changes observed in the glycosidic dihedral angles where each of the seven pyranose units has a different preference in the tilting range (Figure 2) [mean C1-O4′-C4′-C3′ angles for CD·*para*-TS and CD·*meta*-TS have a range of 125.1–131.0 and 114.3–150.2°, respectively]. Whereas, binding at the bottom rim does not show these trends. This indicates at the top rim the induced-fit effect operated by the CD is *better* in adapting to the shape of the *meta*-TS than to the *para*-TS, thus maximizes the long-range contact between the *meta*-TS and the CD. This conclusion is in agreement with the more negative nonbonded interactions calculated in the CD·*meta*-TS complex [$\Delta\Delta\langle E_{vdw}\rangle = -1.87$ kJ mol^{-1}] (Table 2).

There seems to be a general trend that the primary hydroxyl O6 atoms tend to favor the proximity of the *meta*-TS in the CD·TS complex. Figure 3a, b show the behavior of the dihedral angle O5-C5-C6-O6 during simulations. The statistical bar charts show that there is a tendency for the majority of the primary hydroxyl atoms O6 to point toward the CD cavity [(+)-*gauche*] for both regioisomer CD complexes. However, for the CD·*para*-TS complex, the probability of the O6 atoms pointing away [(−)*gauche*] from the CD cavity is much greater than that observed in the CD·*meta*-TS complex. This may give an indication that when binding at the bottom rim, the *meta*-TS is sterically less demanding than the *para*-TS. In agreement, the van der Waals contribution of the CD·*meta*-TS complex is more negative than in the CD·*para*-TS complex [$\Delta\Delta\langle E_{vdw}\rangle = -4.21$ kJ mol^{-1}] (Table 2). The tendency for the majority of the O6 atoms to point toward the

  0947-6539/03/0904-0955 $ 20.00+.50/0

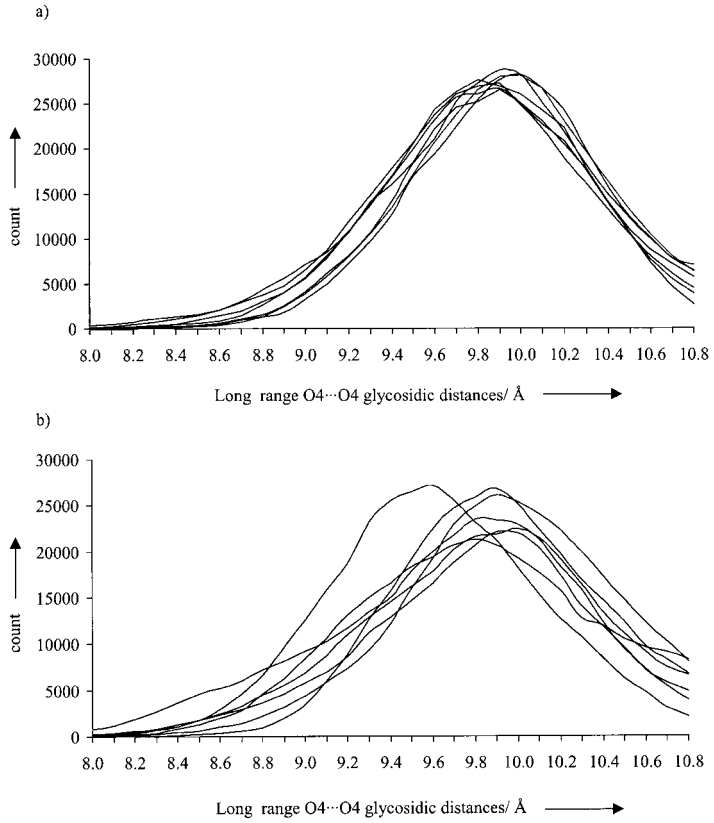

Figure 1. Seven pairs of long-range O4 – O4′ glycosidic distances (each line represents one pair of distances) monitored during one of the 5000 ps MD simulations of a) CD · *para*-TS, and b) CD · *meta*-TS complexes binding at the top, secondary hydroxyl, rim of β-CD. (The graphs are truncated for clarity).

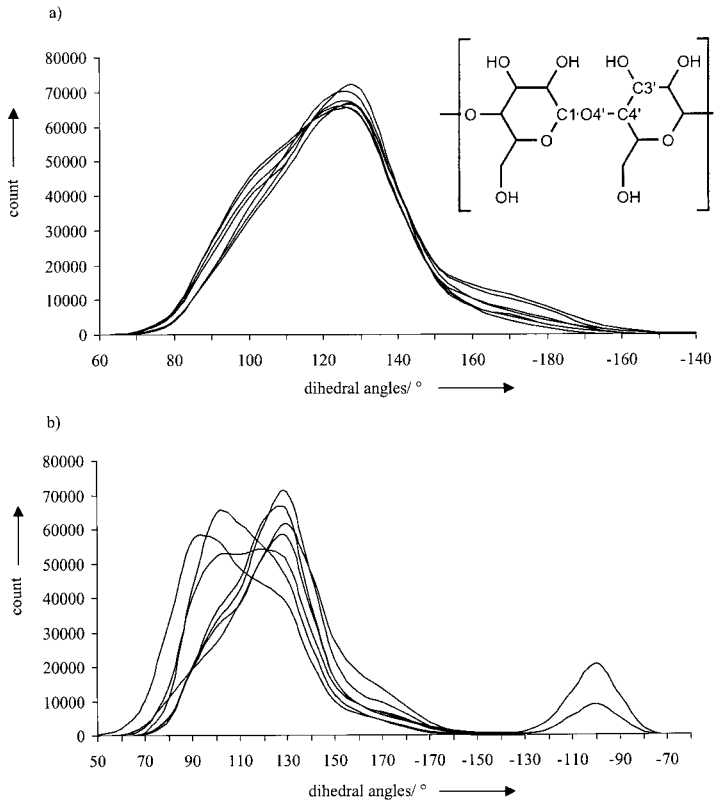

Figure 2. Diagram showing the observed tilting of the seven glycose rings (each line represents one C1-O4′-C4′-C3′ dihedral angle) during one of the 5000 ps MD simulations of a) CD · *para*-TS, and b) CD · *meta*-TS complexes binding at the top, secondary hydroxyl, rim of β-CD. (The graphs are truncated for clarity).

CD cavity means the majority of H6 atoms would be pointing outward. This correlates with the smaller upfield shift observed for H6 compared to H5 in the complex of CD and the *meta* product,[10a] assuming the transition structure and the product bind to CD in a closely related fashion.

The density plot diagrams (Figure 4) show the area sampled by the TS around the top and bottom rim of β-CD during MD simulations; each dot represents the centre of mass of the TS relative to the CD.[18] The large steric bulk of both TSs prevents them from traveling across the cavity and simulations showed that they do not bind deep inside the cavity. Therefore, only shallow binding is necessary for the regioselectivity in this case. Shallow inclusion in molecular recognition has also been suggested in a recent study on the chiral recognition of helical metal complexes by modified CD.[19] The distances between the centre of mass of TS and the centroid of CD were measured for the MD trajectories from the six simulations (Figure 5). As expected, they showed that both TSs bind deeper into the CD cavity from the wider top rim than the narrower bottom rim [mean distance between the centroid of CD and the centre of mass of TS are ≈3.5 Å (top rim) and 5 Å (bottom rim)]. To find the percentage of the TS structure binding deeper in the cavity, we calculated the populations of the TS in the range of 1 – 3 Å and 1 – 4 Å for binding at the top and bottom rims of the CD, respectively. Our results showed that there is a higher population for the *meta*-TS closer to the CD cavity for binding at both rims [for top-rim binding, ≈21% of the *meta*-TS versus ≈14% for the *para*-TS; for bottom-rim binding: ≈14% (*meta*-TS) versus ≈7% (*para*-TS)]. These further

0947-6539/03/0904-0956 $ 20.00+.50/0 *Chem. Eur. J.* **2003**, *9*, No. 4

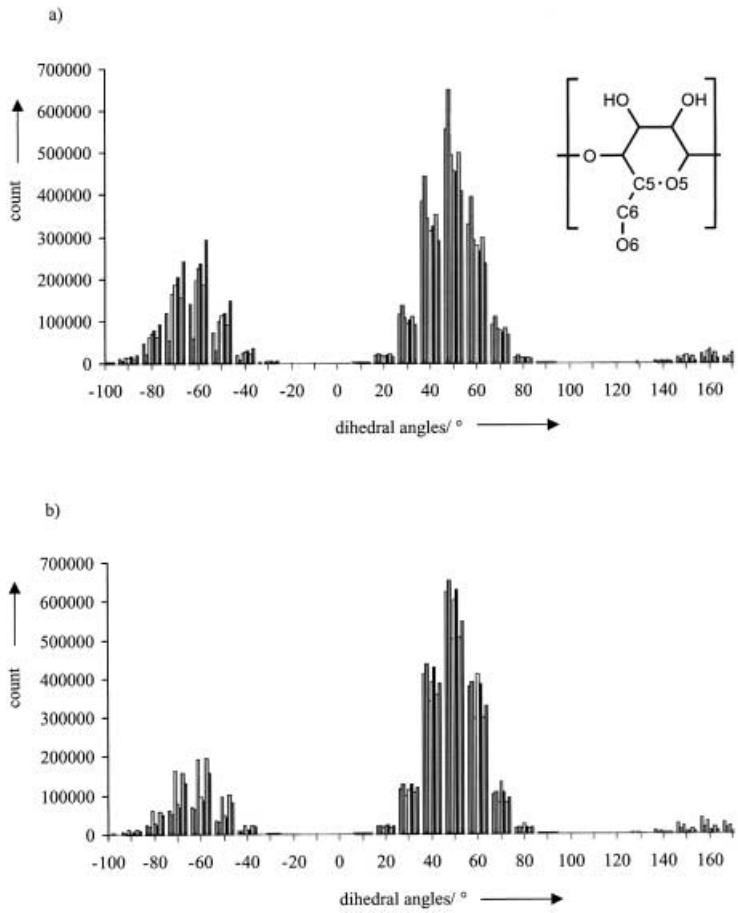

Figure 3. Bar charts showing the changes observed in the seven dihedral angles O5-C5-C6-O6 during the six combined MD simulations. a) CD·*para*-TS, and b) CD·*meta*-TS complexes binding at the bottom, primary hydroxyl, rim of β-CD.

reinforced the conclusion that the *meta*-TS has a better shape complementarity with the CD cavity.

We used Figures 1–3 to examine the differences in the structural features of the CD upon binding with the two different TSs, and Figures 4 and 5 to show that the binding is essentially shallow. The next step is to find a more detailed spatial relationship of the TS relative to the CD during the MD simulations. The structures sampled during MD simulations were energy-minimized and classified into configuration types by partitioning molecular configuration types into subsets.[20] They can be grouped into six configuration types (**a**–**f**), where the TS is considered as a 3D cube with six sides (Scheme 4). Each type of configuration represents approximately each of the six sides being docked first into the CD cavity. Figures 6 and 7 show the different binding configurations at the top and bottom rims of CD from MD simulations and the lowest energy structures belonging to each configuration type are used in the Figures. The binding configuration initially assumed (see Scheme 2 and configuration type **a** in Figure 6) indeed affords a binding preference for *meta*-TS, as expected. However, from Figure 6 and 7, it can be seen that multiple binding geometries are possible for the TSs. Evaluation of the binding energies of these energy-minimum structures illustrates an important aspect of the binding behavior of these 3D molecules with polar functional groups. Although different binding configurations of the CD·TS complex have a different steric demand from the TS to fit into the CD cavity, there are many favorable binding configurations that are not easily accessible from our intuitive model. In the current case, the most stabilized binding configuration is not the one we have initially assumed in Scheme 2.

The next question we need to ask is: do the energy-minimized structures reflect what we see during the simulations? For binding at the top, secondary hydroxyl, rim of CD, examination of the trajectories during MD simulations showed that the *meta*-TS has a preference for configuration types **a**, **c**, and **f**, whereas the *para*-TS has a preference for **c**, **e**, and **f** in all simulations. These preferences correlate well with the binding energy of complexation of the energy-minimized structures (Figure 6), where these configuration types in their respective CD·TS complexes have a stronger binding energy. However, for complexation at the bottom, primary hydroxyl, rim of CD, the binding preference in the MD trajectories depends on the initial CD·TS geometry in the simulations. Therefore, it is less easy to judge whether the configuration types with lower energies indeed are sampled more fre-

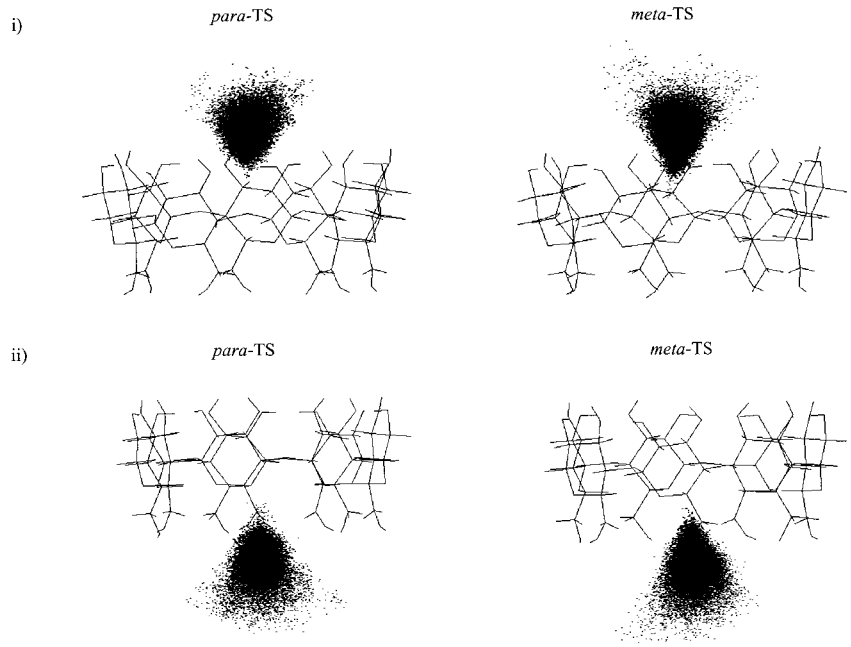

Figure 4. Dot plot diagrams showing the area sampled by the TS around i) the top, secondary hydroxyl, rim, and ii) the bottom, primary hydroxyl, rim of β-CD during MD simulations. Each dot represents the centre of mass of TS relative to β-CD, and the diagrams show the combined 5000 ps MD simulations from six different initial binding configurations.

  0947-6539/03/0904-0957 $ 20.00+.50/0

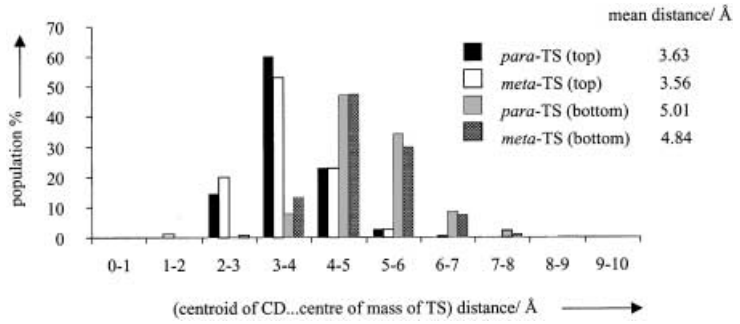

Figure 5. Population analyses of the MD trajectories on the six combined MD simulations for CD·*para*-TS and CD·*meta*-TS for binding at the top and bottom rims of β-CD.

quently than the others. Overall, the disposition of the methyl groups of the *meta*-TS has a larger effect on possible binding modes in complexation with the CD than that in the *para*-isomer. This is reflected in the reduced number of low-energy binding configurations accessible to the *meta*-TS, where configuration types **b** and **e** at the top rim and **b** at the bottom rim were not observed for the CD·*meta*-TS complex from the minimized MD structures.

Since it seems that stability of the minimized low-energy structures in Figures 6 and 7 are related to dominant configurations in MD trajectories, we then used them to find whether there is a direct relationship between the stability of the minimized CD·TS complexes and product selectivity. In the first step of the reaction, methyl-*p*-benzoquinone is loosely complexed within β-CD and simulations showed the molecule is shuttling back and forth within the rims of CD with the possibility of the reactive ene group being exposed at both rims.[11] When isoprene is added into this solution, it can compete for the hydrophobic cavity from both sides. The direction of the approaching isoprene towards the rims determines the type of regioisomer formed. Our results indicate that there is a *correlation* between *meta* product selectivity and a higher number of binding configurations favoring the formation of the CD·*meta*-TS complex. For the bottom rim (Figure 7), the calculated ΔE_{bind} indicate configuration types **a**, **c**, **d**, **e**, and **f** favor the CD·*meta*-TS complex formation over the CD·*para*-TS, and for the top rim (Figure 6) these configurations are **a**, **c**, **d**, and **f**. Basically, the low-energy CD·*meta*-TS complexes shown in Figures 6 and 7 are all lower in energy than the CD·*para*-TS complex of the same configuration type.

In our calculations, we have taken account of the basic problem of shape difference of the *para*- and *meta*-TS, but have not considered how the CD can affect the formation of the Diels–Alder TS; the possibility of an earlier or later TS formation was not considered. Since the simulations show that both TSs are too bulky to fit into the cavity and only shallow binding is needed to produce product selectivity, the small size variation as a consequence of a earlier or later TS may have limited effect upon our results. It is noted that, during MD simulations, the binding of the TS is even shallower than those depicted in the minimized lowest energy structures. Thus, CD-mediated reactions can occur at the periphery of the CD near the boundary between the highly polar aqueous medium and the relatively hydrophobic CD cavity. It has been shown that, even when the substrate complexed with CD lies in heterogeneous environment, the rate of reaction of

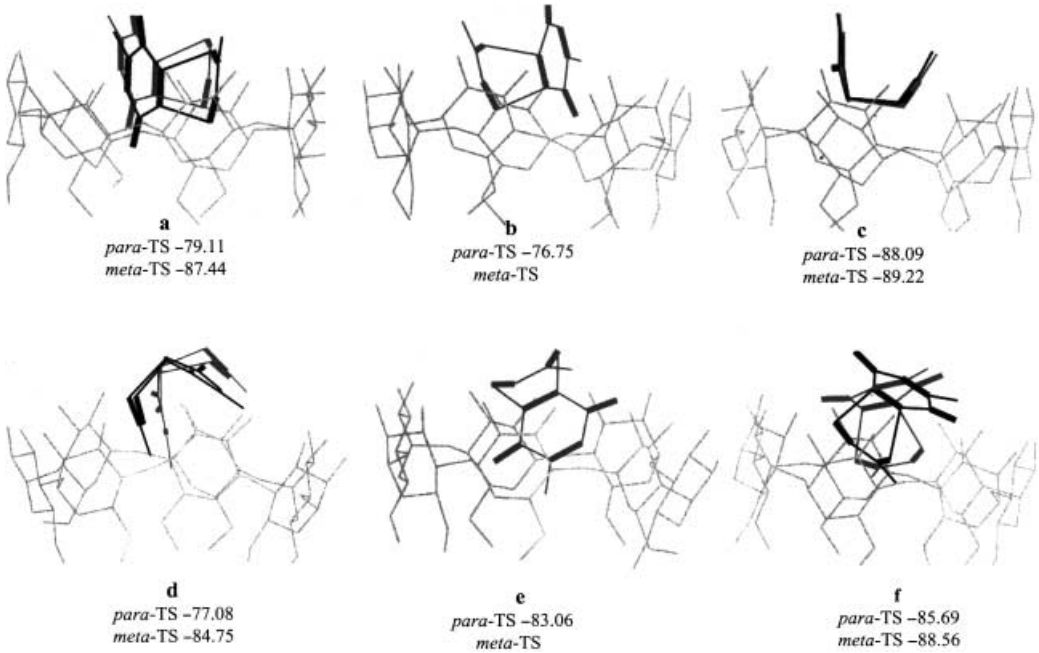

Figure 6. Lowest energy structures of each configuration type (**a**–**f**) of the CD·TS complex binding at the **top rim** minimized from six 5000 ps MD trajectories. – indicates that the configuration was not found within 12.54 kJ mol^{-1} of the global minimum. Values listed below are binding energies [kJ mol^{-1}]. H atoms are omitted for clarity (Black = *meta*-TS, grey = *para*-TS).

0947-6539/03/0904-0958 $ 20.00+.50/0 *Chem. Eur. J.* **2003**, *9*, No. 4

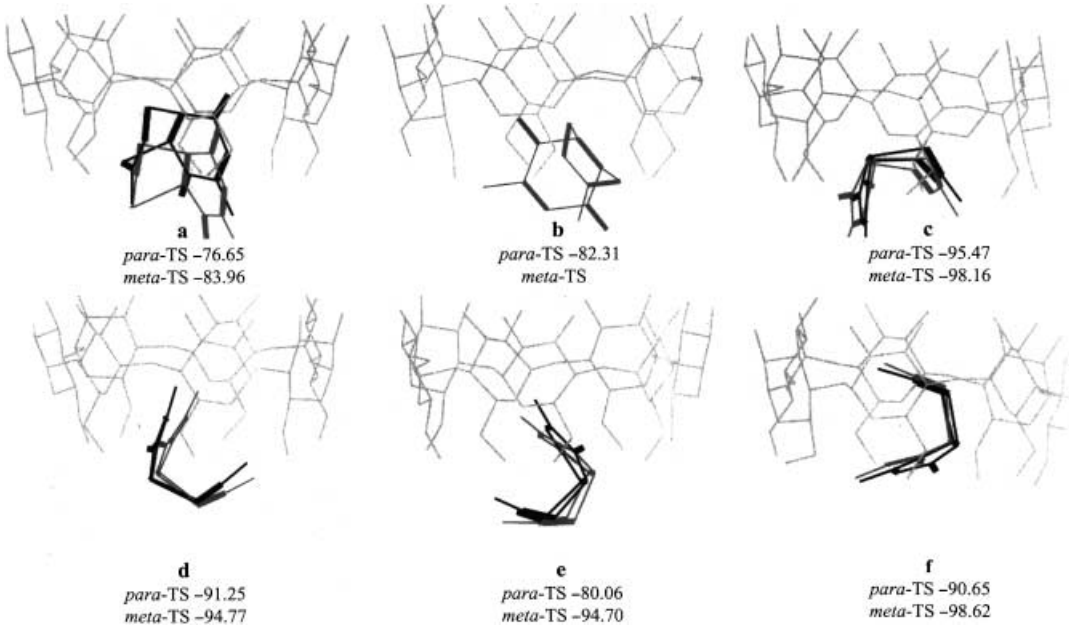

Figure 7. Lowest energy structures of each configuration type (**a–f**) of the CD·TS complex binding at the **bottom rim** minimized from six 5000 ps MD trajectories. – indicates that the configuration was not found within 12.54 kJ mol^{-1} of the global minimum. Values listed below are binding energies [kJ mol^{-1}]. H atoms are omitted for clarity (Black = *meta*-TS, grey = *para*-TS).

CD-catalyzed decaboxylation can be accelerated by lowering the reaction activation from the microsolvation effect of CD cavity.[9e]

Modeling of heptakis-[6-*O*-(2-hydroxy)propyl]-β-CD (7-β-CD): Attempts have been made to modify the structure of β-CD in order to improve the regioselectivity of the product by increasing the depth of the CD cavity, as reported by Chung et al.[10a] However, when heptakis-[6-*O*-(2-hydroxy)-propyl]-β-CD was used in the reactions, almost no selectivity was observed. From the insights we have obtained from the above simulations, it can be clearly seen that the CD cavity can only partially encapsulate the TS. Therefore, deepening the cavity has a limited benefit with respect to enhancing the product selectivity. Moreover, the bottom rim of the CD is an important site for product selectivity in our case. Substituting more bulky hydroxypropyl groups can result in the blocking of the most product-selective site. A 5000 ps MD simulation was carried out to monitor the dynamic behavior of the modified CD. Indeed, snapshots from the MD trajectories show a blocked entrance to the bottom rim. This is reflected in the angle distributions of the seven O5-C5-C6-O6 dihedral angles in the MD trajectories of modified and unmodified β-CD (Figure 8). For the unmodified CD, most dihedral angles can switch between (+)-*gauche* and (−)-*gauche* conformations (Figure 8b). However, for the modified CD, the presence of hydroxypropyl chains have locked three of the O5-C5-C6-O6 dihedral angles in the (−)-*gauche* conformation (pointing away from the cavity) during the 5000 ps MD simulation; in Figure 8a, three bars scoring high in the (−)-*gauche* region are missing in the (+)-*gauche* region, thus leaving only four bars observed in the (+)-*gauche* region (pointing into the cavity). Meanwhile, two dihedral angles were largely locked in the (+)-*gauche* conformation. Although the bottom rim is blocked, according to our previous simulations, low *meta*-selectivity can take place at the wider top rim. However, our simulation shows a more restricted CD upon modification, as shown in Figure 9a; the seven dihedral angles C1-O4′-C4′-C3′ show different preferences in the tilting of the glucose units, in contrast to similar dihedral angle distributions observed in unmodified CD (Figure 9b). As a result, the induced-fit ability of β-CD to complement with the *meta*-TS binding at the top rim is reduced upon modification. This explains why almost no selectivity was observed with modified β-CD.

Conclusion

In this study, we focused on how the effect of shape difference in transition states could affect regioselectivity of CD-mediated Diels–Alder reactions of methyl-*p*-benzoquinone and isoprene. MD simulations with multiple starting guest orientations showed larger binding preference for *meta*-TS and thus agreed with the observed *meta*-product selectivity. The use of a combination of MD and clustering techniques allowed us to have a closer look at the complexation pattern of CD·TS-activated complexes that leads to product selectivity. Several binding configurations have been recognized, and we observed a correlation between *meta*-product selectivity and a greater number of binding configurations of the *meta*-TS favored by β-CD. We also found several interesting features that should be of general interest. Firstly, the binding contribution from the narrower bottom primary hydroxyl rim of CD is often overlooked mainly because the assumption that cyclodextrin inclusion complexes usually formed from the wider top, secondary hydroxyl, rim. In the presence of a bulky guest molecule containing polar functional groups, interaction with the bottom rim of the CD could produce better binding

  0947-6539/03/0904-0959 $ 20.00+.50/0

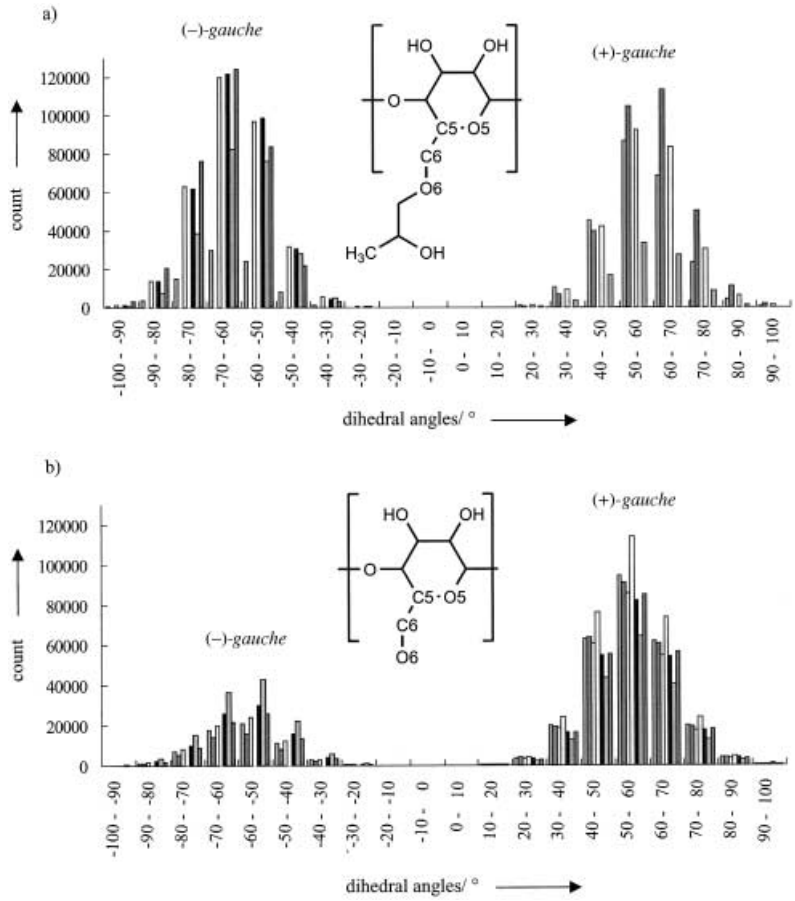

Figure 8. Bar charts showing the dynamic behavior of the seven dihedral angles O5-C5-C6-O6 during a 5000 ps MD simulation at 300 K of a) heptakis-[6-*O*-(2-hydroxy)propyl]-β-CD and b) β-CD.

than with the wider top rim. The second significant observation from our computations is that CD-mediated reactions can occur with shallow binding at the periphery of the CD in the boundary between the highly polar aqueous medium and the relatively hydrophobic cavity. With the above insights obtained from the CD·TS complexes and MD simulations of the modified heptakis-[6-*O*-(2-hydroxy)propyl]-β-CD, we were able to explain why a low selectivity was observed when the Diels–Alder reaction was carried out in this modified CD. Because of the shallow binding characteristics of our CD·TS complexes, deepening the cavity is not a proper strategy to enhance product selectivity. Moreover, some of the hydroxypropyl groups blocked the most selective binding site, the bottom, primary hydroxyl, rim of the CD. Meanwhile, upon modification, the CD cavity became less flexible thus reducing the induced-fit ability to complement with the shape of the *meta*-TS that was observed with the unmodified β-CD.

Computational Methods

Molecular mechanics (MM) and stochastic molecular dynamics (MD) simulations were performed with MacroModel V. 6.5.[21] The all-atom AMBER* force field[21, 22] was used with simulations carried out in the gas phase and/or in the continuum GB/SA model[23] for water. Constant dielectric treatment was used to estimate electrostatic interactions. For the simulation of bimolecular CD·guest complexes, extended nonbonded cutoff distances were set to 20 Å for the van der Waals and electrostatic interactions. The initial geometry of the β-CD was taken from neutron diffraction crystal data of the undecahydrate β-CD,[24] with the water molecules removed and the geometry optimized in the continuum model.

The structures of methyl-*p*-benzoquinone (**1**) and the Diels–Alder transition structures (TS) (*meta*-TS and *para*-TS) were obtained by means of ab initio quantum mechanical calculations. Restricted Hartree–Fock (RHF) method with the 6-31G* basis set was used for geometry optimizations with GAUSSIAN 94.[25] The transition structures were verified by harmonic vibrational frequency analyses where each transition structure has only one imaginary vibrational frequency. Both the *endo* and the *exo* transition structures were calculated (see the Supporting Information), and the results obtained showed that the *endo*-TS are $\approx 8\,kJ\,mol^{-1}$ lower in energy than the *exo*-TS. Although the regioproducts *meta*-**2** and *para*-**2** (Scheme 1) could not give any indication which transition structure is involved in the mechanism, another related substituted benzoquinone gave the *endo* isomer as the main product.[10c–e] For β-CD to contribute to the control of product regioselectivity, it has to differentiate the different methyl dispositions in *meta*- and *para*-TS. The *endo*-TS is U-shaped and the relatively close proximity of the methyl groups makes it possible for β-CD to differentiate between *meta*- and *para*-TS through complexation. In the elongated S-shaped *exo*-TS, the methyl groups are well-separated at the two ends. On account of the finite cavity size of β-CD, complexation of a methyl group at one end is less likely to be affected by the methyl group at the other end, which is exposed in solution. Thus, in our subsequent MM and MD calculations, we focused on *endo*-TS. Default parameters in AMBER* were used for all atoms; however, charges for the TSs were obtained from CHELPG electrostatic potential fitting with Gaussian 94 at the HF/6-31G* level (constrained to reproduce the dipole moment). Throughout the simulations, the geometries of the TSs were kept rigid, except for the methyl substituents which were allowed to freely rotate.

Starting geometry of the CD·guest complex for MCMM and MD simulations was obtained either by docking the guest molecule manually into the CD cavity by means of BumpCheck implemented in MacroModel, or from a docking process. The docking process was carried out by first defining a centroid for the guest molecule and for the CD (calculated as the mean of the seven glycosidic O atoms). The origin was placed at the centroid of the CD with the glycosidic oxygen atoms in the *xy* plane and the docking direction of the guest molecule on the *z* axis. The guest molecule was originally placed 15 Å away from the center of the CD, and after each constrained MM minimization with the distance of guest fixed, the guest molecule was moved by an increment of 1 Å towards the CD. When the guest molecule was in the proximity of the CD, the step size was decreased to 0.5 Å. The CD molecule was held rigid during the docking process. After the starting geometries had been obtained by the docking process, the CD was fully flexible in the subsequent simulations.

Modeling of methyl-*p*-benzoquinone (1)·β-CD complex: Optimized geometries of the CD·**1** complex obtained from docking were used as the

0947-6539/03/0904-0960 $ 20.00+.50/0 *Chem. Eur. J.* **2003**, *9*, No. 4

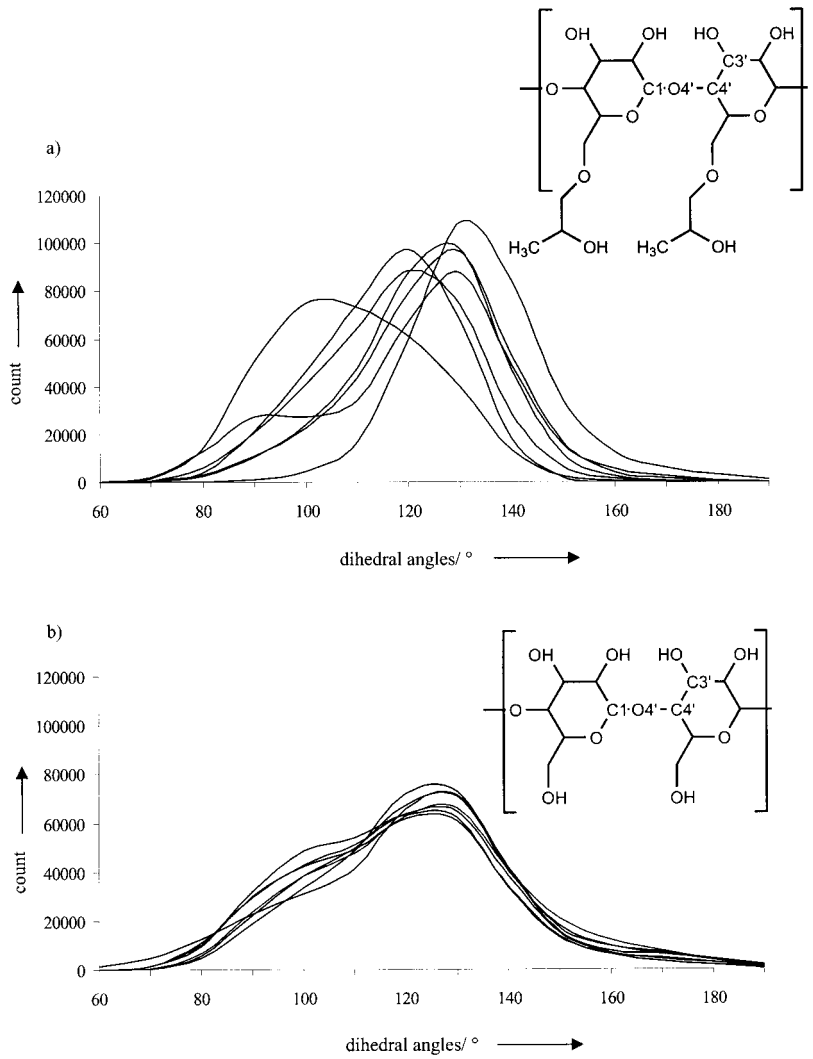

Figure 9. The dynamic behavior of the seven dihedral angles C1-O4′-C4′-C3′ during a 5000 ps MD simulation of a) heptakis-[6-*O*-(2-hydroxy)propyl]-β-CD and b) β-CD.

starting geometries for MD simulations. X-ray crystal structures of simple mono- and disubstituted aromatic molecules reveal that they form inclusion complexes with CD in two basic orientations: head-in and tail-in. Thus in our simulations, two initial docking orientations were considered in the inclusion process (Scheme 3). Stochastic dynamics simulations were carried out in two consecutive runs with the SHAKE protocol implemented in MacroModel. The preliminary equilibration run involved 200 ps integration with 1.5 fs time steps at constant temperature of 300 K. The simulation time of the actual MD run was 1000 ps with 1.5 fs time step, and structures were collected at 2 ps steps.

Modeling of CD·*para*-TS and CD·*meta*-TS complexes: Two types of method were used to explore low energy structures of the CD·TS complexes: the Monte Carlo multiple minimum method (MCMM) and MD simulation. It was found that multiple starting guest orientations have to be used to ensure the binding configuration space of the guest molecule within the CD cavity was adequately explored. Six different initial TS binding orientations at the top and bottom rims of the CD (Scheme 4) were used with the TS considered to be cube with six sides.

MCMM method: Low-energy configurations of the bound CD·TS bimolecular complex were searched by MCMM/MOLS method in MacroModel,[26] with random changes in the molecular position of the guest molecule within the binding site of the CD. Increments of 0–1.0 Å for the translation of the guest molecule and 5–40° for the rotation of the guest molecule around the *x*, *y*, and *z* axes of the CD were used. After each MC step, the structure was minimized by means of the Polak–Ribiere conjugate gradient method,[27] which was also used for the subsequent MC step provided the structure was within 100 kJ of the current global minimum. A total of 1500 MC steps were used for each search.[28] The resulting minimum-energy complex structures were sorted by energy, and the unique structures within a 50 kJ mol^{-1} energy window above the global minimum were stored. During the search, no constraints were applied to the geometry of the CD. The obtained complexes within 12.54 kJ mol^{-1} (3 kcal mol^{-1}) of the global minimum of each set of data were sorted by the clustering program XCluster,[20a] and the configurations were grouped into different configuration types. This allows an easy interpretation of the geometric binding preference and to evaluate the energy contributions. Six basic binding configuration types were found at the top and bottom rims of the CD molecule. They are defined by considering the TS as a 3D cube with six sides, and each binding configuration represents approximately each one of the six sides being docked first into the CD cavity. To look at the fluctuation of the energy of the CD for a given configuration, short MD simulations were carried out on the lowest energy structures belonging to each configuration found in MCMM. It was found that simulations carried out at 273 K with a 30 ps equilibration time followed by a 30 ps averaging time could maintain the configuration of the complex during the MD simulations. At elevated temperatures, such as that described in the next section, interconversion of configuration types takes place.

MD method: MD simulations at 5000 ps with different initial configurations of the CD·TS complexes (Scheme 4) docked at top and bottom rims of β-CD were carried out in a water continuum solvation model and in the gas phase. A 200 ps equilibration step with a 1.5 fs time step was used followed by 5000 ps MD run with 1.5 fs time step at 300 K to obtain ensemble averages. Structures were sampled at regular intervals (1 ps) during the simulations. The sampled structures were energy-minimized by means of the Polak–Ribiere conjugate gradient method and structures within 12.54 kJ mol^{-1} of the global minimum of each data set were used for clustering analysis. The aim of these simulations was to sample the potential energy surface (PES) around the two rims of the CD cavity. However, a problem was encountered with some of the simulations carried out at the bottom rim, where the TS guest molecule escaped from the CD and sampled sites outside the cavity region. This was solved by replacing the desired starting configuration with that obtained from other MD simulations, where a better starting host geometry for a specific configuration was obtained.

MD simulations of β-CD and heptakis-[6-*O*-(2-hydroxy)propyl]-β-CD (7-β-CD): To compare the structural characteristics of heptakis-[6-*O*-(2-hydroxy)propyl]-β-CD to the parent β-CD, we carried out >MD simulations of the two compounds in the water continuum GB/SA model at a constant temperature of 300 K. Equilibration time of 100 ps at 1.5 fs time step followed by 5000 ps at 1.5 fs time steps were used.

  0947-6539/03/0904-0961 $ 20.00+.50/0

Acknowledgements

This research is supported by Academia Sinica, and by generous allocation of computer time by the National Center of High-Performance Computing and the Academia Sinica Computing Center. We thank Dr. T.-S. Hwang for writing the program for the dotplot diagram.

[1] a) G. Wenz, *Angew. Chem.* **1994**, *106*, 851; *Angew. Chem. Int. Ed. Engl.* **1994**, *33*, 803; b) C. J. Easton, S. F. Lincoln, *Chem. Soc. Rev.* **1996**, 163; c) A. P. Croft, R. A. Bartsch, *Tetrahedron* **1983**, *39*, 1417; d) W. Saenger, *Angew. Chem.* **1980**, *92*, 343; *Angew. Chem. Int. Ed. Engl.* **1980**, *19*, 344; e) for the latest reviews, see the special edition of cyclodextrin chemistry in *Chem. Rev.* **1998**, *98*, 1741 – 2076.

[2] a) E. Cervello, C. Jaime, *J. Mol. Struct. (Theochem)* **1998**, *428*, 195; b) A. Entrena, C. Jaime, *J. Org. Chem.* **1997**, *62*, 5923; c) M. Fathallah, F. Fotiadu, C. Jaime, *J. Org. Chem.* **1994**, *59*, 1288; d) P. M. Ivanov, C. Jaime, *J. Mol. Struct. (Theochem)* **1996**, *377*, 137; e) P. M. Ivanov, D. Salvatierra, C. Jaime, *J. Org. Chem.* **1996**, *61*, 7012; f) C. Jaime, J. Redondo, F. Sanchez-Ferrando, A. Virgili, *J. Org. Chem.* **1990**, *55*, 4772; g) F. Perez, C. Jaime, X. Sanchez-Ruiz, *J. Org. Chem.* **1995**, *60*, 3840; h) D. Salvatierra, C. Jaime, A. Virgili, F. Sanchez-Ferrando, *J. Org. Chem.* **1996**, *61*, 9578.

[3] a) M. E. Amato, K. B. Lipkowitz, G. M. Lombardo, G. C. Pappalardo, *J. Chem. Soc. Perkin Trans. 2* **1996**, 321; b) M. E. Amato, K. B. Lipkowitz, G. M. Lombardo, G. C. Pappalardo, *Magn. Reson. Chem.* **1998**, *36*, 693; c) K. B. Lipkowitz, *J. Org. Chem.* **1991**, *56*, 6357; d) K. B. Lipkowitz, S. Raghothama, Y. Jia-an, *J. Am. Chem. Soc.* **1992**, *114*, 1554; e) K. B. Lipkowitz, B. Coner, M. A. Peterson, A. Morreale, *J. Phys. Org. Chem.* **1997**, *10*, 311; f) K. B. Lipkowitz, G. Pearl, B. Coner, M. A. Peterson, *J. Am. Chem. Soc.* **1997**, *119*, 600.

[4] a) H.-J. Schneider, N. K. Sangwan, *J. Chem. Soc. Chem. Commun.* **1986**, 1787; b) N. K. Sangwan, H.-J. Schneider, *J. Chem. Soc. Perkin Trans. 2* **1989**, 1223; c) D. C. Rideout, R. Breslow, *J. Am. Chem. Soc.* **1980**, *102*, 7817; d) D. D. Sternbach, D. M. Rossana, *J. Am. Chem. Soc.* **1982**, *104*, 5853; e) H.-J. Schneider, N. K. Sangwan, *Angew. Chem.* **1987**, *99*, 924; *Angew. Chem. Int. Ed. Engl.* **1987**, *26*, 896; f) S. Otto, W. Blokzijl, J. B. F. N. Engberts, *J. Org. Chem.* **1994**, *59*, 5372; g) A. Meijer, S. Otto, J. B. F. N. Engberts, *J. Org. Chem.* **1998**, *63*, 8989.

[5] a) E. Alvira, C. Cativiela, J. I. Garcia, J. A. Mayoral, *Tetrahedron Lett.* **1995**, *36*, 2129; b) E. Alvira, J. A. Mayoral, J. I. Garcia, *Chem. Phys. Lett.* **1997**, *271*, 178; c) S. P. Kim, A. G. Leach, K. N. Houk, *J. Org. Chem.* **2002**, *67*, 4250.

[6] a) M. Kitagawa, H. Hoshi, M. Sakurai, Y. Inoue, R. Chujo, *Bull. Chem. Soc. Jpn.* **1988**, *61*, 4225; b) M. Sakurai, M. Kitagawa, H. Hoshi, Y. Inoue, R. Chujo, *Bull. Chem. Soc. Jpn.* **1989**, *62*, 2067.

[7] a) E. Junquera, M. Martin-Pastor, E. Aicart, *J. Org. Chem.* **1998**, *63*, 4349; b) T. Kozar, C. A. Venanzi, *J. Mol. Struct. (Theochem)* **1997**, *395 – 396*, 451; c) J. M. Madrid, F. Mendicuti, W. L. Mattice, *J. Phys. Chem. B* **1998**, *102*, 2037; d) J. M. Madrid, F. Mendicuti, W. L. Mattice, *J. Phys. Chem. B* **1998**, *102*, 2037; e) F. M. Menger, M. J. Sherrod, *J. Am. Chem. Soc.* **1988**, *110*, 8606; f) M. Ohashi, K. Kasatani, H. Shinohara, H. Sato, *J. Am. Chem. Soc.* **1990**, *112*, 5824; g) M. Stodeman, U. Berg, A. Svensson, *J. Chem. Soc. Faraday Tans.* **1998**, *94(12)*, 1737; h) C. A. Venanzi, P. M. Canzius, Z. Zhang, J. Bunce, *J. Comput. Chem.* **1989**, *10*, 1038.

[8] I. Tabushi, *Acc. Chem. Res.* **1982**, *15*, 66.

[9] a) F. M. Menger, M. J. Sherrod, *J. Am. Chem. Soc.* **1988**, *110*, 8606; b) H.-J. Thiem, M. Brandl, R. Breslow, *J. Am. Chem. Soc.* **1988**, *110*, 8612; c) V. B. Luzhkov, C. A. Venanzi, *J. Phys. Chem.* **1995**, *99*, 2312; d) V. Luzhkov, J. Åqvist, *J. Am. Chem. Soc.* **1998**, *120*, 6131; e) T. Furuki, F. Hosokawa, M. Sakurai, Y. Inoue, R. Chujo, *J. Am. Chem. Soc.* **1993**, *115*, 2903.

[10] a) W.-S. Chung, J.-Y. Wang, *J. Chem. Soc. Chem. Commun.* **1995**, 971, and references therein; b) M.-M. Yang, MS Thesis, National Chiao Tung University, **1996**; c) G. S. Linz, A. S. Zektzer, G. E. Martin, *J. Org. Chem.* **1988**, *53*, 2647; d) I.-M. Tegmo-Larsson, M. D. Rozeboom, K. N. Houk, *Tetrahedron Lett.* **1981**, *22*, 2043; e) S. Arseniyadis, R. Rodriguez, D. V. Yashunsky, J. Camara, G. Ourisson, *Tetrahedron Lett.* **1994**, *35*, 4843.

[11] See the Supporting Information: Figure showing snapshots taken during MD simulations from the two guest orientations in Scheme 3.

[12] a) For reviews see H. J. Schneider, F. Hacket, V. Rüdiger, H. Ikeda, *Chem. Rev.* **1998**, *98*, 1755; b) L. Szejtli, *Cyclodextrin Technology*, Kluwer Academic, Dordecht (The Netherlands), **1988**; c) R. Bergeron in *J. Inclusion Compounds*, *Vol. 3* (Eds.: J. L. Atwood, J. E. D. Davies, D. D. MacNicol), Academic, London, **1984**, pp. 391 – 443; d) D. Hallén, A. Schön, I. Shehatta, I. Wadsö, *J. Chem. Soc. Faraday Trans.* **1992**, *88*, 2859.

[13] R. I. Gelb, L. M. Schwartz, R. F. Johnson, D. A. Laufer, *J. Am. Chem. Soc.* **1979**, *101*, 1869.

[14] E. Zitha-Bovens, H. van Bekkum, J. A. Peters, F. G. C. Geraldes, *Eur. J. Inorg. Chem.* **1999**, 287.

[15] P. D. Ross, M. V. Rekharsky, *Biophys. J.* **1996**, *71*, 2144.

[16] M. V. Rekharsky, M. P. Mayhew, R. N. Goldberg, P. D. Ross, Y. Yamashoji, Y.Inoue, *J. Phys. Chem. B* **1997**, *101*, 87.

[17] Z.-P. Yi, H.-L. Chem, Z.-Z. Huang, Q. Huang, J.-S. Yu, *J. Chem. Soc. Perkin Trans. 2* **2000**, 121.

[18] All MD trajectories were moved to a common coordinate axis followed by 3D superposition to display in mutual orientations. The transition structure from each trajectory is represented by a dot calculated from the center of mass of the TS relative to the centroid of the best-fit plane defined by the seven acetal-linking oxygen atoms of the CD, and the CD structure displayed in the diagram is calculated from the average of all the trajectories. The program for the above operations was written by Dr. T.-S. Hwang.

[19] K. Kano, H. Hasegawa, *J. Am. Chem. Soc.* **2001**, *123*, 10616.

[20] a) P. S. Shenkin, D. Q. McDonald, *J. Comput. Chem.* **1994**, *15*, 899; b) R. R. Sokol, Clustering and Classification: Background and Current Directions, in J. Van Ryzin, *Classification and Clustering*, Academic Press, New York, **1977**.

[21] MacroModel, Interactive Molecular Modeling System, Version 6.5, BatchMin, Columbia University, NY.

[22] a) S. J. Weiner, P. A. Kollman, D. A. Case, U. C. Singh, C. Chio, G. Alagona, S. Profeta, P. Weiner, *J. Am. Chem. Soc.* **1984**, *106*, 765; b) S. J. Weiner, P. A. Kollman, D. A. Case, *J. Comput. Chem.* **1986**, *7*, 230.

[23] a) W. C. Still, A. Tempczyk, R. C. Hawley, T. Hendrickson, *J. Am. Chem. Soc.* **1990**, *112*, 6127; b) D. Qiu, P. S. Shenkin, F. P. Hollinger, W. C. Still, *J. Phys. Chem. A* **1997**, *101*, 3005; c) J. Weiser, A. A. Weiser, P. S. Shenkin, W. C. Still, *J. Comput. Chem.* **1998**, *19*, 797; d) J. Weiser, A. A. Weiser, P. S. Shenkin, W. C. Still, *J. Comput. Chem.* **1998**, *19*, 1110.

[24] C. Betzel, W. Saenger, B. E. Hingerty, G. M. Brown, *J. Am. Chem. Soc.* **1984**, *106*, 7545.

[25] Gaussian 94 (Revision D.4), M. J. Frisch, G. W. Trucks, H. B. Schlegel, P. G. A. Gill, J. A. Montgomery, Jr., A. L. K. Raghavachari, V. G. Zakrzewski, J. V. Ortiz, J. B. Foresman, J. Cioslowski, B. B. Stefanov, A. Nanayakkara, M. Hallacombe, C. Y. Peng, P. Y. Ayala, W. Chen, M. W. Wong, J. L. Andres, E. S. Replogle, R. Gomperts, R. L. Martin, D. J. Fox, J. S. Binkley, D. J. Defrees, J. Blake, J. P. Stewart, M. S. Gordon, C. Gonzalez, and J. A. Pople, Gaussian, Inc., Pittsburgh PA, **1995**.

[26] G. Chang, W. C. Guida, W. C. Still, *J. Am. Chem. Soc.* **1989**, *111*, 4379.

[27] E. Polak, G. Ribiere, *Revue Francaise Inf. Rech. Oper.* **1969**, *16-R1*, 35.

[28] A total of 9000 MCMM/MOLS steps (from searches with six starting configurations) were carried out at each rim of the CD. Although the number of search steps we used were not many, we have observed that for each search most unique structures found at later steps had a higher energy and also a larger number of structures with lower energy were duplicates of previously found structures.

Received: August 7, 2002 [F4328]

